RSC Advances

ROYAL SOCIETY OF CHEMISTRY

www.rsc.org/advances

Reactive-template fabrication of porous NiO nanowires for electrocatalytic O_2 evolution reaction

Palanisamy Manivasakan, Parthiban Ramasamy and Jinkwon Kim*

Department of Chemistry and GETRC, Kongju National University,
182, Shinkwondong, Kongju, 314-701, Chungnam-do, Republic of Korea

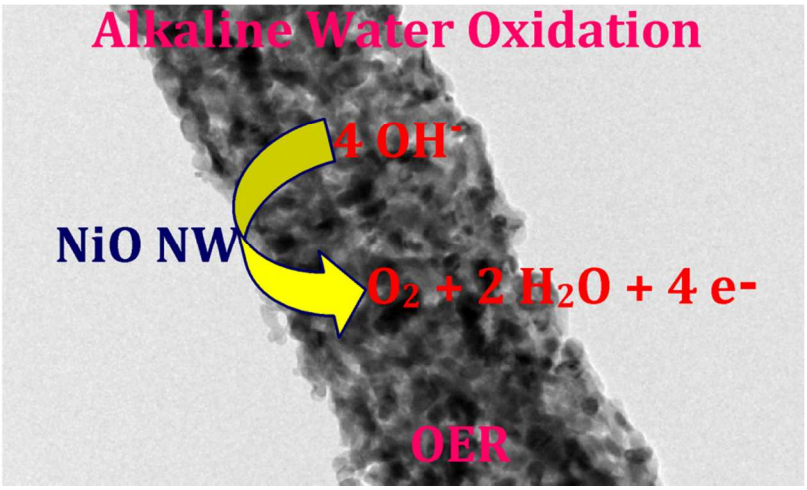

Macro-mesoporous NiO nanowire was demonstrated as an active electrocatalyst for O_2 evolution reaction in alkaline media.

Cite this: DOI: 10.1039/c0xx00000x

www.rsc.org/xxxxxx

ARTICLE TYPE

Reactive-template fabrication of porous NiO nanowires for electrocatalytic O_2 evolution reaction†

Palanisamy Manivasakan, Parthiban Ramasamy, and Jinkwon Kim*

Received (in XXX, XXX) Xth XXXXXXXXX 20XX, Accepted Xth XXXXXXXXX 20XX

DOI: 10.1039/b000000x

One-dimensional nickel oxide nanowires (NiO NWs) with lengths of ~8 µm and widths of ~100 nm were synthesized by a reactive-template directed solvothermal route using selenium nanowires (Se NWs) as the sacrificial template. Electrocatalytic O_2 evolution reaction (OER) was studied on polycrystalline NiO NWs using cyclic voltammetry (CV) and linear sweep voltammetry (LSV) measurements in alkaline media. Nickel oxide nanoparticles (NiO NPs) with size distributions of 50-100 nm were also synthesized by facile hydrothermal method for comparative electrocatalytic evaluation with the porous NiO NWs. In the present case we demonstrate the applicability of spin coating technique to fabricate the porous NiO NWs on fluorine doped tin oxide (FTO) glass electrode. The porous NiO NWs coated FTO (NiO NWs/FTO) exhibit higher electrocatalytic activity and higher current efficiency of OER than that of NiO NPs coated FTO (NiO NPs/FTO). The electrocatalytic properties of the NiO NWs are discussed in the context of earlier reports based on NiO catalyst. The as-prepared NiO NWs represents a new class of non-precious catalysts for OER, which demonstrates promise for future applications in alkaline water splitting.

1. Introduction

Alkaline water splitting is a potential candidate for alkaline electrolysers, solar hydrogen cells and alkaline fuel cells[1-2]. In alkaline water electrolyser, electrocatalytic OER is the most important anode reaction in which molecular oxygen (O_2) is generated by water oxidation in alkaline media. Economical alkaline water electrolyser demands active, stable and cost-effective electrocatalyst for water oxidation reaction with activity similar to platinum. In general, platinum (Pt) is an efficient catalyst for the OER while ruthenium (Ru) and iridium (Ir) oxides are also known to act as best catalysts for OER. Thus, precious catalysts based on Pt, Ir, and Ru alloys have been employed for the best OER activity in fuel cells.[3] Both electrocatalytic performance and catalyst cost seem to be major criteria in the design of cost-effective alkaline water electrolyser with high efficiency.

Research concerning non-precious metal oxide nanostructures has attracted considerable interest due to their contribution to the development of efficient alkaline water electrolyser.[3-6] Gorlin et al.[3] demonstrated the nanostructured manganese oxide (Mn_xO_y) thin films as an active catalyst for OER in alkaline media. Thereafter, much attention has focused on the development of nanostructured metal oxide catalysts based on non-precious metals such as Mn, Fe, Co, and Ni for OER. Nanostructured amorphous metal oxide films containing Fe, Co, and Ni have gained significant attention for their role in catalyzing the OER. It represents the OER activities of binary and ternary mixed metal oxide combinations based on Fe, Co, and Ni.[7] Electrochemically deposited Ni based oxide nanostructures such as NiO_x, $NiCeO_x$, $NiCoO_x$, $NiCuO_x$, $NiFeO_x$, and $NiLaO_x$ have been revealed as the active heterogeneous electrocatalysts for the OER.[8] Among them, NiO nanostructures are recognized as an active and robust non-precious electrocatalyst for OER in alkaline media.[9,10] Furthermore, the specific OER characteristics of a graphene supported Ni nanostructures has demonstrated in literature.[11]

Currently, there is a growing interest in the development of non-precious electrocatalyst based on the porous nanostructures with different dimensions.[12] Besides enlarge surface area of the porous nanostructures, nano-confined space offers unique environment for electrochemical reactions. On the other hand, particles size and shape distributions limit the overall property of the catalysts in nanoscale catalysts. Moreover, it is ultra-small metal oxide particles with high surface to volume ratio and uniform size distributions are difficult to synthesis and store. Long time storage of ultra-small particles (<10 nm) usually leads to aggregation, which can critically affect the electrocatalytic performances of catalysts. Furthermore, 1D metal oxide nanostructures composed of ultrafine particles show their unique catalytic properties. Recent reports are available on the synthesis of 1D metal oxide nanostructures with uniform composition, size and shape.[13,14] However, the reports are rare on the synthesis and electrocatalytic applications of porous NiO NWs. It still remains a challenge to attain porous NiO NWs with long uniform length and high surface area for electrocatalytic OER.

In this work, we explore the synthesis of porous NiO NWs composed of ultra-fine NiO particles via chemical conversion of

nickel selenide nanowires ($Ni_{0.85}Se$ NWs) in static air atmosphere. Herein, we demonstrate a facile reactive-template strategy to fabricate uniform, polycrystalline NiO NWs with porosity. The proposed solvothermal route is simple, convenient and effective to obtain porous NiO NWs with high surface area. The possible mechanism for the synthesis and conversion of $Ni_{0.85}Se$ NWs into NiO NWs are proposed. The as-prepared porous NiO NWs exhibit excellent electrocatalytic activity to OER. We also compare the catalytic performance of NiO NWs with NiO NPs. The porous NiO NWs show better electrochemical activity than the NiO NPs.

2. Experimental

2.1 Materials

Sodium selenite (Na_2SeO_3), ascorbic acid ($C_6H_8O_6$), 3-mercaptopropionic acid (MPA), nickel (II) chloride hexahydrate ($NiCl_2.6H_2O$) and Nafion perfluorinated ion-exchange resin (eq. wt. 1100) 5 wt. % in mixture of lower aliphatic alcohols and water (45%) were purchased from Sigma-Aldrich. Ethanol and methanol were purchased from Samchun Pure Chemicals Co. Ltd., Korea. Ultra pure water (18 MΩ cm) was obtained from a micro pure HIQ water purifying system. Fluorine doped tin oxide coated glass electrode with resistivity of ~8 Ω/sq. (FTO; geometrical area 5×5 mm) received from Sigma-Aldrich was used for the electrochemical studies.

2.2 Synthesis of 1D $Ni_{0.85}Se$ NWs and NiO NWs

Se NWs were prepared by a modified literature procedure.[15] The porous NiO NWs were synthesized by the reactive-template directed solvothermal route using 1D Se NWs as a sacrificial template, which was based on our earlier work.[16] In a typical synthesis, 40 mg Se NWs were dispersed in 50 mL of absolute ethanol and treated with 1 mL mercaptopropionic acid (MPA). The carboxylic (hydrophilic) and thiol groups of MPA render excellent dispersibility and dispersion stability for Se NWs. Subsequently, 0.5 mmol of $NiCl_2•6H_2O$ was dissolved in 20 mL of absolute ethanol and added slowly into the MPA-stabilised Se NWs dispersion under sonication. Then, 5 mL of ultra-pure water was added to the mixture and sonicated at room temperature for 1 h. The reaction mixture was transferred into a 100 mL Teflon-lined autoclave and maintained at 120 °C for 12 h and then cooled to room temperature. The excess MPA and unreacted precursors were removed by repeated washing with ethanol prior to chemical conversion. After purification, the sample was dried under vacuum and annealed in static air at 500 °C for 2 h to produce porous NiO NWs. The procedure for the synthesis of plate-like NiO NPs is given in ESI†.

2.3 Characterizations

X-ray diffraction (XRD) measurements were performed using a Rigaku MiniFlex II X-ray diffractometer. The surface morphology and chemical compositions of the $Ni_{0.85}Se$ NWs and NiO NWs were obtained using field emission scanning electron microscopy (FE-SEM, Hitachi S-4800 UHR) with a Bruker energy dispersive (EDX) system, at an accelerating voltage of 3 kV. The elemental composition of the NiO NWs and its chemical and electronic states were examined using X-ray photoelectron spectroscopy (XPS, Multilab ESCA 2000). Transmission electron microscopy (TEM) and high-resolution TEM (HRTEM) images with selected area electron diffraction (SAED) patterns were recorded on a JEM-2100F instrument (JEOL, Japan) at an accelerating voltage of 200 kV. The Brunauer-Emmett-Teller (BET) surface area and porosity profiles of NiO NWs were determined using a BELSORP specific surface area and pore size analyzer (BEL Japan, Inc.). All the electrochemical measurements were carried out with a Metrohm Autolab electrochemical workstation (PGSTAT 302N, The Netherlands) in a three electrode cell arrangement.

2.4 Electrochemical measurements

The electrocatalytic activity for the OER was studied with the linear sweep and cyclic voltammetric technique using a bare or modified FTO as the working electrode, glassy carbon as the counter electrode, and Ag/AgCl as the reference electrode in a conventional three-electrode cell. Before the sample was modified, FTO was cleaned and washed with nitric acid/acetone (1:1) and ultra pure water in an ultra sonicator bath. The pre-cleaned FTO was dried using a high-purity nitrogen spray. Subsequently, 25 mg of the catalyst and 100 µL Nafion solutions were ultrasonically dispersed in 900 µL of water/methanol (1:1) solution and then the dispersion was ultrasonicated for 15 min to obtain a homogeneous solution of catalyst ink. Then, 50 µL of catalyst ink was carefully coated on the pre-cleaned FTO surface using spin coating technique and dried at 30°C for 5 h to obtain the porous NiO NWs coated FTO electrode (NiO NWs/FTO). The catalyst loading was constant (50 µL) for all experiments. The protocol was precisely repeated for the construction of NiO NPs modified electrode (NiO NPs/FTO). All the cyclic voltammetry (CV) experiments were carried out at room temperature in 0.1 M KOH solution. Prior to the electrochemical measurements, the electrodes were cycled at 50 mV s^{-1} between 0 and 600 mV under a saturated nitrogen atmosphere until reproducible cyclic voltammograms were obtained. LSV curves for the OER were obtained using the NiO NWs and NiO NPs-coated FTO electrodes in the potential range 0 - 1000 mV in 0.5 M KOH under a saturated oxygen atmosphere. The current density values reported (mA cm^{-2}) are based on geometric area of the FTO. The profiles of the oxygen overpotential measurements for OER were provided in ESI†.

3. Results and Discussions

The synthesized power samples of Se NWs, $Ni_{0.85}Se$ NWs, and NiO NWs were analyzed through the powder X-ray diffraction as shown in Fig. 1. The elemental compositions of the $Ni_{0.85}Se$ NWs are given in Fig. S1.† The composition of $Ni_{0.85}Se$ NWs was remained at 300 °C, but oxidized to NiO by annealing

at 500 °C in air for 2 h. It can be deduced from the Scherrer's formula[17] that the crystallite sizes of NiO NWs (average ~11.5 nm) are smaller than those of $Ni_{0.85}Se$ NWs (average ~20 nm). Apparently, the chemical conversion of hexagonal $Ni_{0.85}Se$ NWs into cubic NiO NWs contributes reduction in crystallite size.

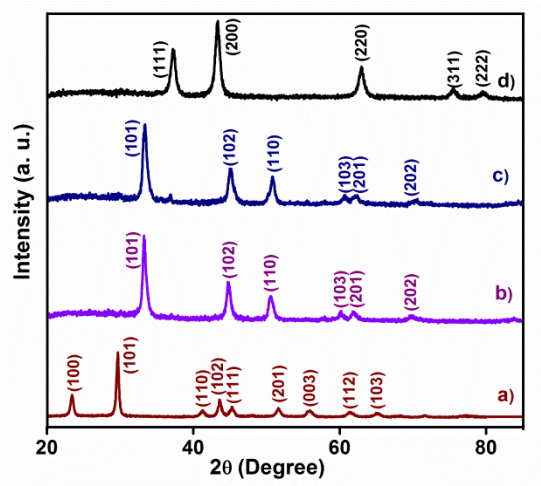

Fig. 1 XRD patterns of (a) Se NWs, (b) $Ni_{0.85}Se$ NWs synthesized at 120°C, (c) $Ni_{0.85}Se$ NWs after annealing at 300°C and (d) NiO NWs after annealing at 500°C.

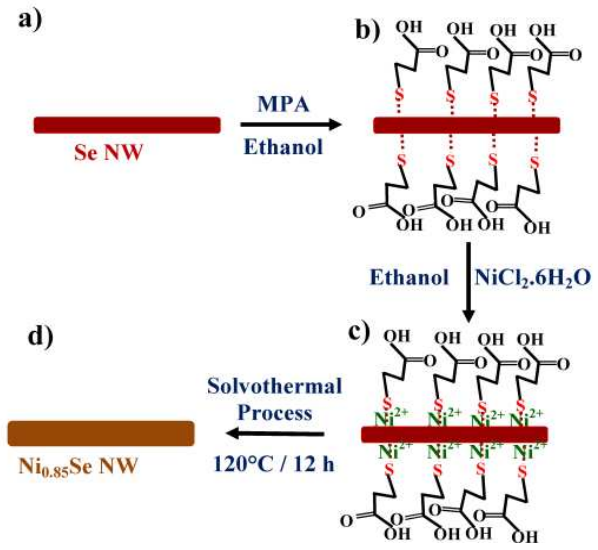

Scheme 1 Schematic diagrams for the formation of the hexagonal $Ni_{0.85}Se$ NWs. (a) Se NWs; (b) MPA stabilized Se NWs; (c) Nickel ions functionalized Se NWs; and (d) $Ni_{0.85}Se$ NWs.

The formation of hexagonal $Ni_{0.85}Se$ NWs and its chemical conversion strategy to cubic NiO NWs are illustrated in Scheme 1 and 2. Initially, the thiol group of MPA can strongly interact with the surface of Se NWs,[18] which facilitates the functionalization of Ni^{2+} ions on the surface of Se NWs through the coordination of carboxylate groups. During the solvothermal process, the Ni^{2+} ions located at the surface are reacting with the Se NWs to form the hexagonal $Ni_{0.85}Se$ NWs (Scheme 1). Sublimation-controlled oxidation reaction is expected to occur readily ($Ni_{0.85}Se$ + 3/2 O_2 ➔ NiO + SeO_2) when $Ni_{0.85}Se$ NWs are exposed to static air atmosphere at 500 °C (Scheme 2). During the thermal oxidation process, the NiO shell was formed on the surface of the $Ni_{0.85}Se$ NWs with Kirkendall voids at the interface which results from the non-equilibrium interdiffusion.[19,20] The release of internally generated SeO_2 from the $Ni_{0.85}Se$ nanocrystals drives the formation of highly porous NiO NWs with high surface area.

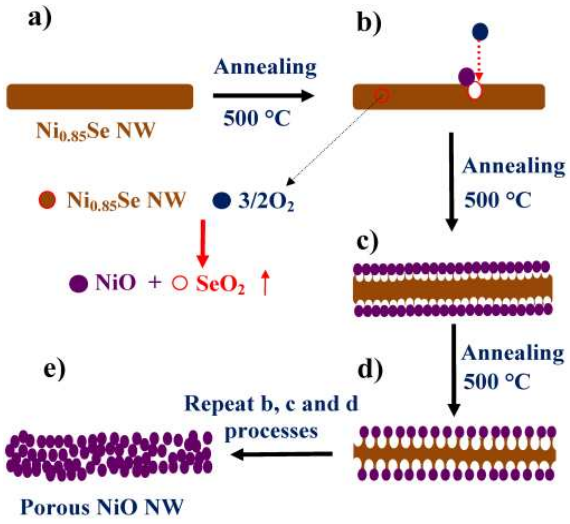

Scheme 2 Schematic diagram for the chemical conversion of $Ni_{0.85}Se$ NWs into NiO NWs. (a) $Ni_{0.85}Se$ NWs; (b) interaction of oxygen with $Ni_{0.85}Se$ NWs; (c) NiO shell on the surface of $Ni_{0.85}Se$ NWs in the thermal oxidation process; (d) porous NiO shell on the surface of $Ni_{0.85}Se$ NWs; and (e) highly porous NiO NWs.

The characterization of the nickel valence states and the elemental composition of the NiO NWs were performed using XPS analysis (Fig. 2). There are no peaks related to Se or SeO_2, but peaks only of pure NiO. In Fig. 2b, the two major peaks centered at 854.5 and 872.4 eV with two shake-up excitations (satellite peaks) at 860.5 and 878.8 eV are indexed to the Ni $2p_{3/2}$ and Ni $2p_{1/2}$ peak positions of NiO, respectively. These values are consistent with the literature values for divalent nickel oxide.[21] The high resolution O1s spectrum of the NiO NWs (Fig. 2c) displayed two oxygen contributions marked as 1 and 2. Component 1 centered at 529.2 eV is a typical metal-oxygen bond of Ni-O in NiO[22,23] and component 2 at 530.7 eV is assigned to nickel hydroxide and surface hydroxyl groups.[22,23]

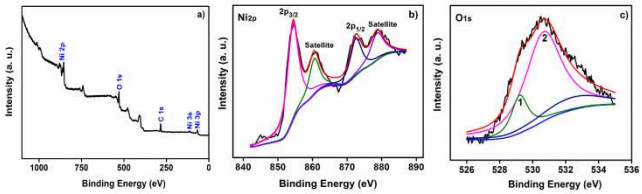

Fig. 2 XPS spectrum of the porous NiO NWs. (a) Full scan; (b) Ni_{2p} core levels; and (c) O_{1s} core levels.

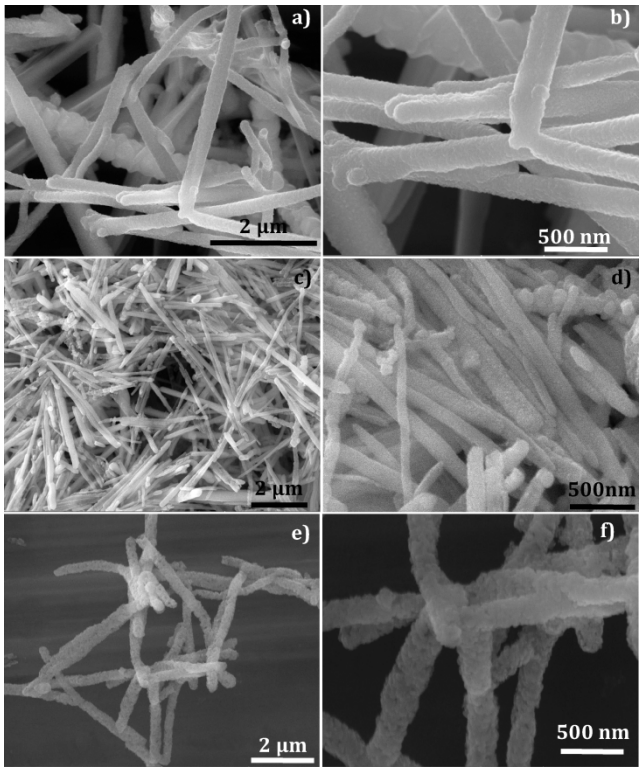

Fig. 3 FE-SEM images of (a, b) $Ni_{0.85}Se$ NWs, (c, d) $Ni_{0.85}Se$ NWs after annealing at 300°C and (e, f) NiO NWs after annealing at 500°C.

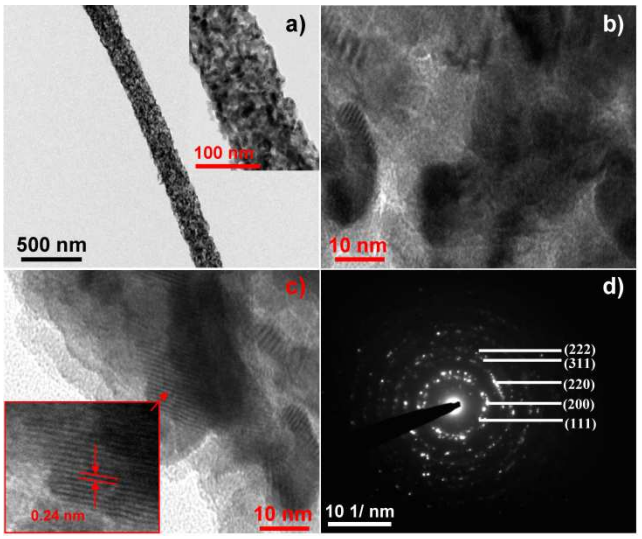

Fig. 4 TEM images of porous NiO NWs. (a) TEM image; (b, c) HRTEM image; and (d) SAED pattern.

Samples at three representative stages (120, 300, and 500 °C) were examined by FE-SEM. It is obviously revealed from FE-SEM images that the chemical conversion of $Ni_{0.85}Se$ into NiO follows 1D to 1D transformation, indicating this synthetic method strictly controls the dimensionality and morphology of the nanomaterials. As displayed in Fig. 4, TEM and HRTEM images show that the NiO nanowires are highly porous, composed of nanocrystallites of 10-20 nm in size and pores with similar size. The nanowires are crystalline as revealed in Fig. 4c with lattice fringes with spacing of 0.24 nm which corresponds to the (111) lattice plane of NiO. The ring patterns of SAED support the polycrystalline nature of the NiO NWs.

The specific surface area of NiO NWs estimated from the BET plot (Fig. S2, ESI†) is 120 $m^2 g^{-1}$ and it showed a typical porous structure with total pore volume of 0.36 $cm^3 g^{-1}$ and average pore diameter of 12 nm. Nitrogen adsorption-desorption isotherm and pore-size distribution plot for the synthesized NiO NWs are shown in Fig. 5. The general shape of the nitrogen adsorption-desorption isotherm showed a typical IUPAC type IV pattern with an H3 hysteresis loop, indicating the presence of open slit-shaped mesopores.[24] However, the adsorption branch of isotherm closely resemble type II pattern, suggesting the existence of macropores.[25] The Barrett-Joyner-Halenda (BJH) distribution plot was displayed in Fig. 5b. The corresponding pore size distribution obtained by the BJH plot shows the presence of mesopores (2-50 nm) in addition to macropores ranging from 50 to 180 nm. In contrast, HRTEM and BET average pore diameter analysis are closely supports the distribution of mesopores. This suggests that the two or more NiO nanowires are interpenetrating and interlinking to form few macropores during the annealing process. It can be revealed from surface area and pore size analysis that the obtained textural features are quite good for enhanced mass transport property.[26] The plate like nickel oxide nanoparticles (NiO NPs) with size distributions of 50-100 nm were also synthesized for comparative electrocatalytic evaluation with the porous NiO NWs. The XRD and FE-SEM profiles of NiO NPs are given in Fig. S3.† Nitrogen adsorption-desorption isotherm for the synthesized NiO NPs are shown in Fig. S4.† As synthesised NiO NPs own the specific surface area of 83 $m^2 g^{-1}$ with total pore volume of 0.32 $cm^3 g^{-1}$ and average pore diameter of 16 nm.

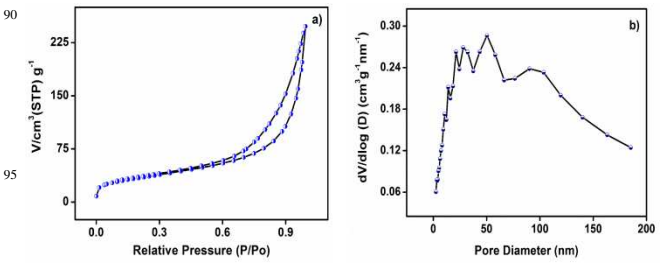

Fig. 5 (a) Nitrogen adsorption-desorption isotherm and (b) pore-size distribution plot for synthesized NiO NWs.

The bare FTO and the NiO NWs-modified electrode (NiO NWs/FTO) were electrochemically characterized by measuring the CV in 0.1 M KOH which are shown in Fig. 6a. The CV curve of the NiO NWs/FTO shows a redox couple for Ni^{2+}/Ni^{3+} ($Ni(OH)_2/NiOOH$)[27] during the potential scan from 0 to 700 mV while the bare FTO exhibits almost a straight line, conforming the functionalization of the NiO NWs in modified electrode. A pair of current peaks can be clearly identified during the anodic and cathodic sweeps and the peak current density increases with increasing scan rate (Fig. 6b), due to

electrochemical activity of the redox species (Ni^{2+}/ Ni^{3+}) at the electrode surface. As can be seen in Fig. 6c, the peak current density (J_p) exhibits a linear dependence on the scan rate, suggesting the electrode (NiO NWs/FTO) process is surface controlled.[28]

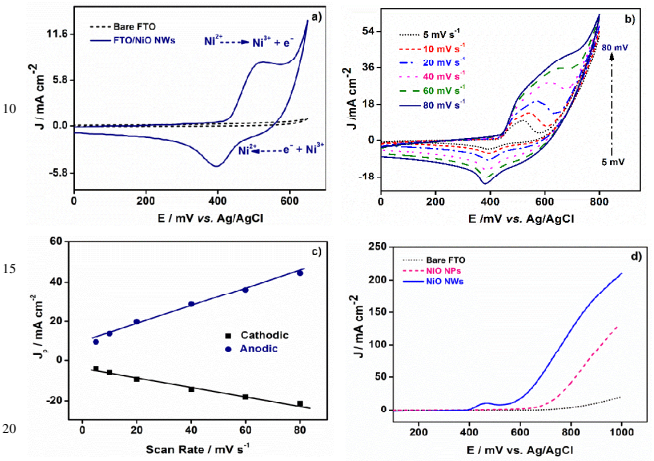

Fig. 6 (a) CV curves of the bare FTO and NiONWs/FTO at 10 mVs^{-1} in 0.1 M KOH, (b) CV curves of NiONWs/FTO at different scan rates in 0.1 M KOH solution saturated with nitrogen, (c) Plots of peak current density *versus* scan rate, and (d) LSV plots of NiO NWs, NiO NPs, and bare FTO electrodes at 10 mV s^{-1} in 0.5 M KOH for OER.

Considering the electrocatalytic behavior of NiO NWs in water electrolyser, the OER activities were investigated using NiO NWs/FTO and NiO NPs/FTO electrodes. For OER (Fig.6d), NiO NWs/FTO shows a high catalytic activity with low onset potential of 560 mV *vs.* Ag/AgCl (overpotential, η = 353 mV), which was nearly 150 mV less positive than the NiO NPs-modified electrode (710 mV *vs.* Ag/AgCl, η = 503 mV). The enhanced textural properties of the NiO NWs likely contributed to the reduction in overpotential of 150 mV, which can facilitate the presence of the appropriate NiO active sites at low overpotential (η = 353 mV) to drive the OER. When comparing the OER activity of NiO NWs and NiO NPs (Fig. 6d), it is obvious that the porous NiO NWs-modified electrode have shown much higher anodic limiting current density (210.53 mA cm^{-2} at 1V *vs.* Ag/AgCl) than the NiO NPs-modified electrode (134.42 mA cm^{-2} at 1V *vs.* Ag/AgCl). This enhancement in the anodic limiting current density can be attributed to more oxygen evolution due to the increase in water oxidation in porous NiO NWs-modified electrode compared to the NiO NPs-modified one. It can be concluded that the improved textural properties (high surface area with increased pore volume and decreased pore diameter) of NiO NWs enables more active sites on electrode surface which implies superior electrocatalytic activity of NiO NWs than NiO NPs.

A convention normally used to judge the OER activity is based on the potential required to oxidize water at a current density of 10 mA cm^{-2}.[3] At a current density of 10 mA cm^{-2}, the NiO NWs/FTO exhibited oxygen overpotential (η) of 363 mV whereas the NiO NPs-modified electrode showed oxygen overpotential (η) of 501 mV. Obviously, the NiO NWs/FTO shows 138 mV reductions in overpotential at a current density of 10 mA cm^{-2} confirming the better OER activity of the porous NiO NWs. This observation reveals that the OER activity of the porous NiO NWs outperforms the electrocatalytic properties of the NiO NPs. Moreover, its OER activity matches or surpasses the activities of the best reported OER catalyst based on non-precious metal oxides.[7] In general, non-precious metal based catalyst system achieved 10 mA cm^{-2} current densities at operating overpotentials between 350 and 430 mV.[8] At a current density of 10 mA cm^{-2}, the fabricated porous NiO NWs (catalyst loading ~1.25 mg) exhibit oxygen overpotential (η) of 363 mV which is very close to lowest overpotential of precious metal-free catalyst system. Hence, the developed porous NiO NWs outperforms the electrocatalytic properties of the NiO_x, CoO_x, $NiCeO_x$, $NiCoO_x$, $NiCuO_x$, and $NiLaO_x$ catalysts system.[8]

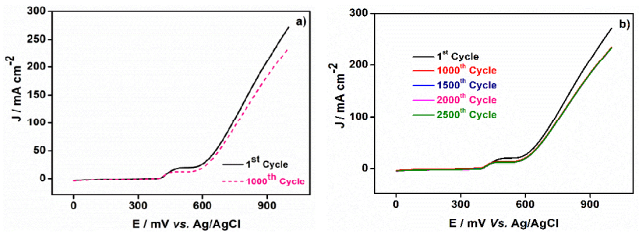

Fig. 7 LSV plots for NiO NWs/FTO before and after CV testing of 1000 cycles (a) and 2500 cycles (b) at 50 mV s^{-1} in 0.5 M KOH.

Fig. 7a displays the linear sweep voltammograms for the NiO NWs/FTO in 0.5 M KOH solution. The performance of the NiO NWs/FTO for the OER slightly decays and the current density (decreased from 271.86 to 234.63 mA cm^{-2}) at 1V vs. Ag/AgCl shows 86% retention after 1000 CV cycles. Fig. 7b presents the number of cycles *vs.* current density shows the electrochemical stability and durability of NiO NWs/FTO for OER activity. Obviously, Fig. 7b confirms that the current density almost stable after 1000 cycles and shows negligible changes up to 2500 cycles. It reveals that the proposed NiO NWs holds better catalytic stability and durability in alkaline media. Thus, the NiO NWs with high surface area deliver the excellent catalytic activity towards OER than the NiO NPs. Hence, the proposed porous NiO NWs will be utilized as an efficient non-precious catalyst for OER activity in AEM-URFCs.

4. Conclusions

In conclusion, we have reported for the new class of porous NiO nanowires consisting of ultra-fine nanocrystals (10-15 nm) and a high density of mesopores, which was synthesized by a reactive-template directed solvothermal route followed by chemical conversion technique. Heat treatment of $Ni_{0.85}Se$

nanowires in an aerobic condition gives NiO nanowires with lengths of ~8 µm and widths of ~100 nm. The developed protocol provides a feasible way to control the dimensionality of the NiO NWs with mesoporous structure. Their high surface area (120 m^2g^{-1}) provides an excellent electrocatalytic behavior towards OER activity compared to NiO NPs. This comparison through different morphology (NWs and NPs) offers strategies to enhance the performance of O_2 electrode reaction in alkaline electrolyser. The developed porous NiO NWs could be used as a new class of catalyst for OER in alkaline electrolysers. More importantly, the as-synthesized porous NiO NWs could be applied in anion exchange membrane-unitized regenerative fuel cells (AEM-URFCs).

Acknowledgements

This work was financially supported by Basic Science Research Program (2012R1A1A2043731) through the National Research Foundation.

Notes and references

Author information

Department of Chemistry and GETRC, Kongju National University, 182, Shinkwondong, Kongju, 314-701, Chungnam-do, Republic of Korea

**Corresponding Author*

E-mail: jkim@kongju.ac.kr, Fax: +82-41-850-8613; Tel: +82-41-850-8496.

Supporting Information

Electronic Supplementary Information (ESI†) available: EDX profile of $Ni_{0.85}Se$ nanowire, BET plot for NiO NWs, BET plot, XRD and FE-SEM data for NiO nanoparticles. See DOI: xxx/xxx/

1. M. Hamdani, R. N. Singh and P. Chartier, *Int. J. Electrochem. Sci.,* 2010, **5,** 556.
2. B. H. R. Suryanto, X. Lu and C. Zhao, *J. Mater. Chem. A,* 2013, **1,** 12726.
3. Y. Gorlin and T. F. Jaramillo, *J. Am. Chem. Soc.,* 2010, **132,** 13612.
4. J. W. Desmond Ng, M. Tang and T. F. Jaramillo, *Energy Environ. Sci.,* 2014, **7,** 2017.
5. J. W. Desmond Ng, Y. Gorlin, T. Hatsukade and T. F. Jaramillo, *Adv. Energy Mater.,* 2013, **3,** 1545.
6. Y. Gorlin, B. L. Kaiser, J. D. Benck, S. Gul, S. M. Webb, V. K. Yachandra, J. Yano and T. F. Jaramillo, *J. Am. Chem. Soc. 2013, **135,** 8525.*
7. R. D. L. Smith, M. S. Prévot, R. D. Fagan, S. Trudel and C. P. Berlinguette, *J. Am. Chem.Soc.,* 2013, **135,** 11580.
8. C. C. L. McCrory, S. Jung, J. C. Peters and T. F. Jaramillo, *J. Am. Chem. Soc.,* 2013, **135,** 16977.
9. A. Singh, S. L. Y. Chang, R. K. Hocking, U. Bachcde and L. Spiccia, *Energy Environ. Sci.,* 2013, **6,** 579.
10. A. Singh, S. L. Y. Chang, R. K. Hocking, U. Bachcde and L. Spiccia, *Catal. Sci. Technol.,* 2013, **3,** 1725.
11. Z. Pu, Q. Liu, A. M. Asiri, X. Sun, *J. Appl. Electrochem.*, 2014, **44,** 1165.
12. J. H. Bae, J. Han and T. D. Chung, *Phys. Chem. Chem. Phys.,* 2012, **14,** 448.
13. Q. Zhang, H.Wang, X. Jia, B. Liu and Y. Yang, *Nanoscale,* 2013, **5,** 7175.
14. P. Wu, H. Zhang, Y. Qian, Y. Hu, H. Zhang and C. Cai, *J. Phys. Chem. C*, 2013, **117,** 19091.
15. Q. Li and V. W.Yam, *Chem. Commun.,* 2006, 1006.
16. P. Ramasamy, D. Lim, J. Kim and J. Kim, *RSC Adv.,* 2014, **4,** 2858.
17. P. Ramasamy, S. I. Mamum, J. Jang and J. Kim, *CrystEngComm,* 2013, **15,** 2061.
18. M. Tiecco, L. Testaferri, C. Santi, C. Tomassini, S. Santoro, F. Marini, L. Bagnoli, A. Temperini and F. Costantino, *Eur. J. Org. Chem.,* 2006, 4867.
19. Y. Ren, W. K. Chim, S. Y. Chiam, J. Q. Huang, C. Pi and J. S. Pan, *Adv. Funct. Mater.,* 2010, **20,** 3336.
20. D. Ha, L. M. Moreau, S. Honrao, R. G. Hennig and R. D. Robinson, *J. Phys. Chem. C*, 2013, **117,** 14303.
21. J. Li, F. Luo, Q. Zhao, Z. Li, H. Yuan and D. Xiao, *J. Mater. Chem. A,* 2014, **2,** 4690.
22. J. R. Manders, S. Tsang, M. J. Hartel, T. Lai, S. Chen, C. M. Amb, J. R. Reynolds and F. So, *Adv. Funct. Mater.,* 2013, **23,** 2993.
23. E. L. Ratcliff, J. Meyer, K. X. Steirer, A. Garcia, J. J. Berry, D. S. Ginley, D. C. Olson, A. Kahn, and N. R. Armstrong, *Chem. Mater.,* 2011, **23,** 4988.
24. K. S. W. Sing, D. H. Everett, R. A. W. Haul, L. Moscou, R. A. Pierotti, J. Rouquerol and T. Siemieniewska, *Pure & Appl. Chem.,* 1985, **57(4),** 603.
25. L. Nie, A. Meng, J. Yu, M. Jaroniec, *Scientific Reports,* 2013, **3,** 3215**.**
26. L. Chen, S. Xu, X. Li, G. Tian, Y. Li, J. C. Rooke, G. Zhu, S. Qiu, Y. Wei, X. Yang, Z. Liu, B. Su, *J. Colloid Interface Sci.,* 2012, **377,** 368-374.
27. A. Elzatahry, *Int. J. Electrochem. Sci.,* 2014, **9,** 22.
28. L. Ren, K. S. Hui and K. N. Hui, *J. Mater. Chem. A,* 2013, **1,** 5689.

